Pergamon

Int. J. Heat Mass Transfer. Vol. 41, No. 10, pp. 1303–1311, 1998

Printed in Great Britain
0017–9310/98 $19.00+0.00

PII: S0017–9310(97)00201–9

Effect of baffle spacing on pressure drop and local heat transfer in shell-and-tube heat exchangers for staggered tube arrangement

HUADONG LI† and VOLKER KOTTKE

Institute of Food Technology, Department of Food Process Engineering, Hohenheim University, 70599 Stuttgart, Germany

(*Received* 18 *November* 1996 *and in final form* 14 *May* 1997)

Abstract—Local heat transfer and pressure drop on the shell side of shell-and-tube heat exchangers with segmental baffles were investigated for different baffle spacings. The distributions of the local heat transfer coefficients on each tube surface within a fully developed baffle compartment were determined and visualized by means of mass transfer measurements. Per-tube, per-row and per-compartment average heat transfer coefficients were drawn from the local values. The local pressure measurements allow the determination of the shell-side flow distributions. For same Reynolds number, the pressure drop and average heat transfer are increased by an increased baffle spacing due to a reduced leakage through the baffle-shell clearance. The experimental results were compared with literature values. © 1998 Elsevier Science Ltd.

INTRODUCTION

The baffles are primarily used in shell-and-tube heat exchangers for supporting the tubes and for inducing cross flow over the tubes, resulting in improved heat transfer performance. In these heat exchangers, the shell-side flow is complicated for two reasons, the first is the approximately sinusoidal overall flow pattern as the fluid flows through the tube bundle, and the second is the influence of the various leakages through the clearances required for the construction of the exchangers. A change in the baffle spacing will affect both the way in which the flow executes the 180° turns and the extent to which true crossflow is achieved relative to the tubes in any compartment. Such spacing-related alternations of the fluid flow affect both the heat transfer and pressure drop characteristics.

The common focus of the published methods for the design of shell-and-tube heat exchangers is to predict the average shell-side heat transfer coefficient and pressure drop [1–6]. In order to define the path toward improved performance of shell-and-tube heat exchangers, Sparrow [7, 8] and Gay [9, 10] have determined the per-tube average heat transfer coefficients in exchangers having no leakage by means of different mass transfer techniques. These distributions of individual tube coefficients gave some insight into the flow patterns on the shell-side, but provided no knowledge about the variation of the local heat transfer coefficients on the tube surfaces.

In this paper, the effect of the baffle spacing between successive baffles on the pressure drop and local heat transfer coefficients is investigated. By means of a mass transfer technique based on absorption, chemical and coupled colour reaction [11–13], the local mass transfer coefficients can be visualized and quantitatively determined. The leakage rate for different baffle spacings and Reynolds numbers, which is obtained from the pressure drop measurement through the clearances, will be presented. The Reynolds number is varied from 500 to 16 000.

EXPERIMENTS

The shell-and-tube heat exchanger used in this work is shown in Fig. 1(a). It consists of (1) a cylindrical plexiglass shell and (2) two removable PVC tube sheets, which support (3) a bundle of glass tubes and (4) eight tie rods. These tie rods adjust the baffle spacing [Fig. 1(e)] and also reduce the bundle bypass stream in the gap between the bundle and the shell wall. The test section is located in the third baffle compartment from the exchanger inlet, which is in the fully developed flow region. Figure 1(b) shows the internal configuration of the heat exchanger. Because of the symmetric tube arrangement, only 20 tubes are presented. Each tube location is denoted by two numbers, the first of these is the number of the row from top to bottom where the tube is located. The second number from left to right indicates the tube position within the row. All of the tubes were made removable and can be replaced by a pressure sensing tube [Fig. 1(c)] or by a mass transfer measuring tube [Fig. 1(d)]. The main dimensions and features of the heat exchangers are given in Table 1. Three baffle spacings (S = 113, 144 and 175 mm) are investigated.

† Author to whom correspondence should be addressed.

NOMENCLATURE

a	pitch ratio	S	baffle spacing [m]
A	flow area $A = D_i S$ [m^2]	u	fluid velocity, $u = \dot{v}/A$ [m s^{-1}]
C_p	specific heat capacity [K J (kg K)$^{-1}$]	u_{eff}	effective fluid velocity, $u_{eff} = Pu$
d	tube outside diameter [m]	u_o	fluid velocity in clearance [m s^{-1}]
D	diameter of baffle hole [m]	$\dot{v}$	inlet flow rate [m^3 s^{-1}]
D_i	inside diameter of the shell [m]	X	length measured from the outer baffle surface parallel to the tube axis [m]
D_1	diameter of baffles [m]	Z	orifice shape factor.
l	characteristic length, $l = \pi d/2$ [m]		
L	distance of two baffle compartments [m]		
Nu	Nusselt number, $Nu = \alpha d/\lambda$	Greek symbols	
P	percentage of the main stream in the cross flow zone relative to the heat exchanger entrance [%]	α	heat transfer coefficient [W (m^2 K)$^{-1}$]
		δ	baffle thickness [m]
		ζ	pressure drop coefficient, $\zeta = (2\Delta P_1/\rho u^2)(d/L)$
ΔP_1	pressure drop in two compartments [N m^{-2}]	ζ_0	pressure drop coefficient, $\zeta_0 = (2\Delta P_2/\rho u_0^2)$
ΔP_2	pressure drop in clearance [N m^{-2}]	λ	thermal conductivity [W (K m)$^{-1}$]
Re	Reynolds number, $Re = ul/(\psi v)$	v	kinematic viscosity [m^2 s^{-1}]
Re_{eff}	effective Reynolds number, $Re_{eff} = u_{eff} l/(\psi v)$	ψ	tube bundle porosity, $\psi = 1 - \pi/(4a)$.

For the visualization and mass transfer measurements, the surface of the mass transfer measuring tube is coated with a wet filter paper containing an aqueous solution of manganese(II)chloride with hydrogen peroxide, and is inserted in the heat exchanger. Air is sucked in by a suction fan. The reaction gas (ammonia) is added as a pulse to the main stream in very low concentration. The colour intensity of the filter paper corresponds to the locally transferred mass and can be evaluated quantitatively by photometrical remission processing. Conversion of the mass transfer results to heat transfer is accomplished by employing the analogy between the two transport processes.

For the measurements of the pressure drop (ΔP_1) in

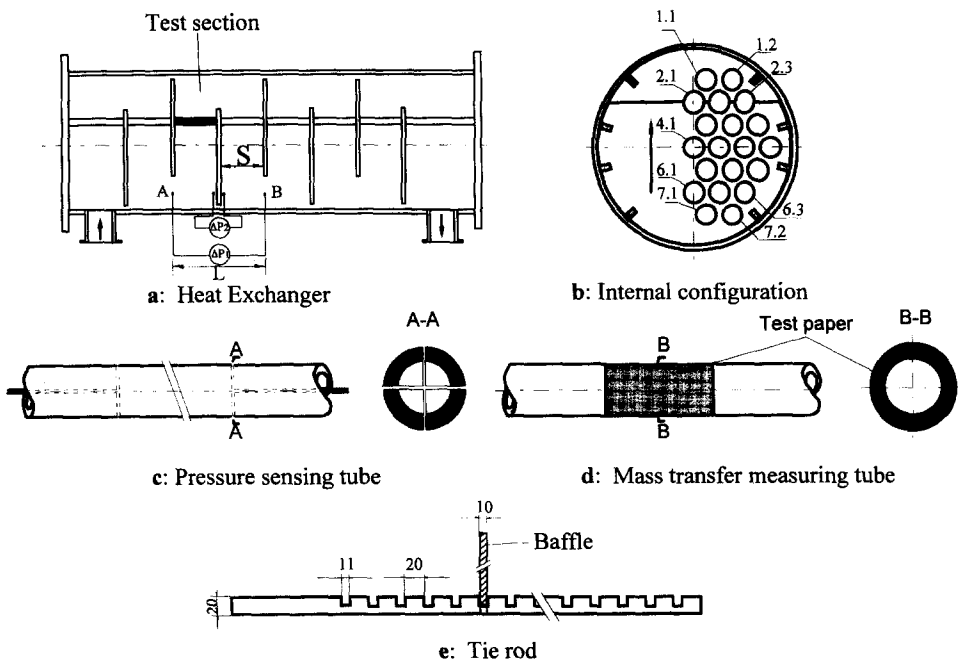

Fig. 1. Construction of the heat exchanger and measuring tubes.

Table 1. Main dimensions and features of the heat exchangers

Item	Dimensions
Inside diameter of shell D_i	290 mm
Diameter of baffle hole D	30.4 mm
Diameter of baffles D_1	286 mm
Outside diameter of tubes d	30 mm
Baffle spacing S	113, 144 and 175 mm
Pitch ratio a	1.26
Baffle cut H	77 mm
Number of tubes	37
Baffle thickness δ	10 mm
Tube arrangement	Staggered

two baffle compartments, the tappings of the pressure sensing tube [Fig. 1(c)] were located at A and B [Fig. 1(a)] under the second and fourth baffle. During the measurements of the pressure drop in the baffle-tube clearances or in the baffle-shell clearance (ΔP_2), the pressure sensing tube was inserted in the positions of the central tubes [2.1, 3.1, 4.1, 5.1, 6.1 and 7.1 Fig. 1(b)] successively, the tappings were located just before and after the third baffle [Fig. 1(a)]. The pressure measurement using a FC014-Micromanometer from Furness Control Ltd has an inaccuracy of about $\pm 2.5\%$.

RESULTS AND DISCUSSION

Heat and mass transfer

Figure 2 shows the photograph of the local mass transfer distribution on the surface of the tube 4.1 situated in the centre of the cross-flow region for $Re = 8000$ and baffle spacing (S) 144 mm. The corresponding three-dimensional distribution of the local Nusselt number is given in this figure, where X is the tube length and line the circumferential position of the tube. From $X = 0$ to $X = 10$ mm in the second baffle, the local mass and heat transfer decrease rapidly as the boundary layer increases in the annular orifice. After the baffle, the local mass and heat transfer coefficients are particularly low due to the zone of local separated flow. From $X = 50$ to $X = 155$ mm, the distribution of the local heat and mass transfer coefficient displays a typical characteristic such as that in the ideal staggered tube bundle [14]. The line 10 in Fig. 2(b) with high coefficients corresponds to the forward stagnation line, the lines 6 and 12 present the separation of the boundary layer in the front portion of the tube. Figure 2 reveals that the local heat transfer coefficients are not uniformly distributed on the tube surface. Owing to the turning of the fluid from one baffle compartment into the next, a large separation zone behind the baffle at the leading edge forms, which leads to a nonuniform longitudinal distribution.

Figure 3(a)–(c) shows the circumferential distributions of the Nusselt numbers averaged over the tube length in the tested baffle compartment at $Re = 8000$ for the three baffle spacings ($S = 113$, 144 and 175 mm), respectively, where the per-tube average Nusselt numbers are also given. Figure 3 provides detailed information not only about the local heat transfer coefficient distributions of all tubes but also about the flow patten in the compartment. The first noteworthy feature of this figure is the similar circumferential distributions at the tubes situated from row 1 to row 6. However, the distributions at tubes 7.1 and 7.2 are totally different from other tubes, because of the dominance of longitudinal directed flow. Therefore, the heat transfer coefficients at these tubes are particularly low. Secondly, the distributions are not affected by the baffle spacing, but the per-tube average Nusselt numbers generally increase with an increasing baffle spacing, especially in the window zone (e.g. at tubes 1.1, 1.2, 7.1 and 7.2), in which the flow velocity at the same Reynolds number increases with increasing baffle spacing depending on the higher flow rate at larger spacing.

The circumferential heat transfer distributions (averaged over the tube length) are more homogeneous as at cylindrical tubes in an ideal tube bundle [14] depending on the separated flow zone behind the baffle.

The effect of the tie rods as sealing strips for the bundle bypass stream in the gap between the bundle and the shell wall can be also observed in Fig. 3, in which four tie rods are located between the tubes 1.2 and 2.3, 3.3 and 4.4, 4.4 and 5.3, and 6.3 and 7.2, respectively [Fig. 1(b)]. The tie rod diverts fluid into the tube bundle, which results in higher heat transfer coefficients on the tube surfaces near the shell wall. In addition, the baffle-shell leakage can also affect the local heat transfer at those shell-adjacent tubes.

To illustrate the effect of the baffle spacing on heat transfer more clearly, the average Nusselt numbers of tubes in the circumferential direction for $Re = 8000$ and the three investigated baffle spacings are plotted in Fig. 4 as a function of the dimensionless tube length $(X-10)/S$, where X is the tube length, 10 the baffle thickness and S the baffle spacing. This figure indicates that the increase of the local heat transfer coefficients is not uniform along the tube, which depends on both the tube position in the bundle and the tube length. The reason for the increase in the heat transfer on the tube 7.1 with the increase in baffle spacing is given above. According to the definition of the Reynolds number, the mean flow velocity in the cross-flow zone should be same, if the leakage is negligible. Owing to change of the leakage, particularly the baffle-shell leakage in these investigated heat exchangers, the actual main flow velocity in the cross-flow zone increases by 4% with the baffle spacing increase from $S = 113$ mm to $S = 175$ mm, which will be later discussed in detail. This is the reason for the increase of the per-tube average heat transfer coefficient in the cross-flow zone, e.g. tube 4.1, with the increase of the baffle spacing.

The per-compartment average Nusselt numbers for different baffle spacings are presented in Fig. 5 as a

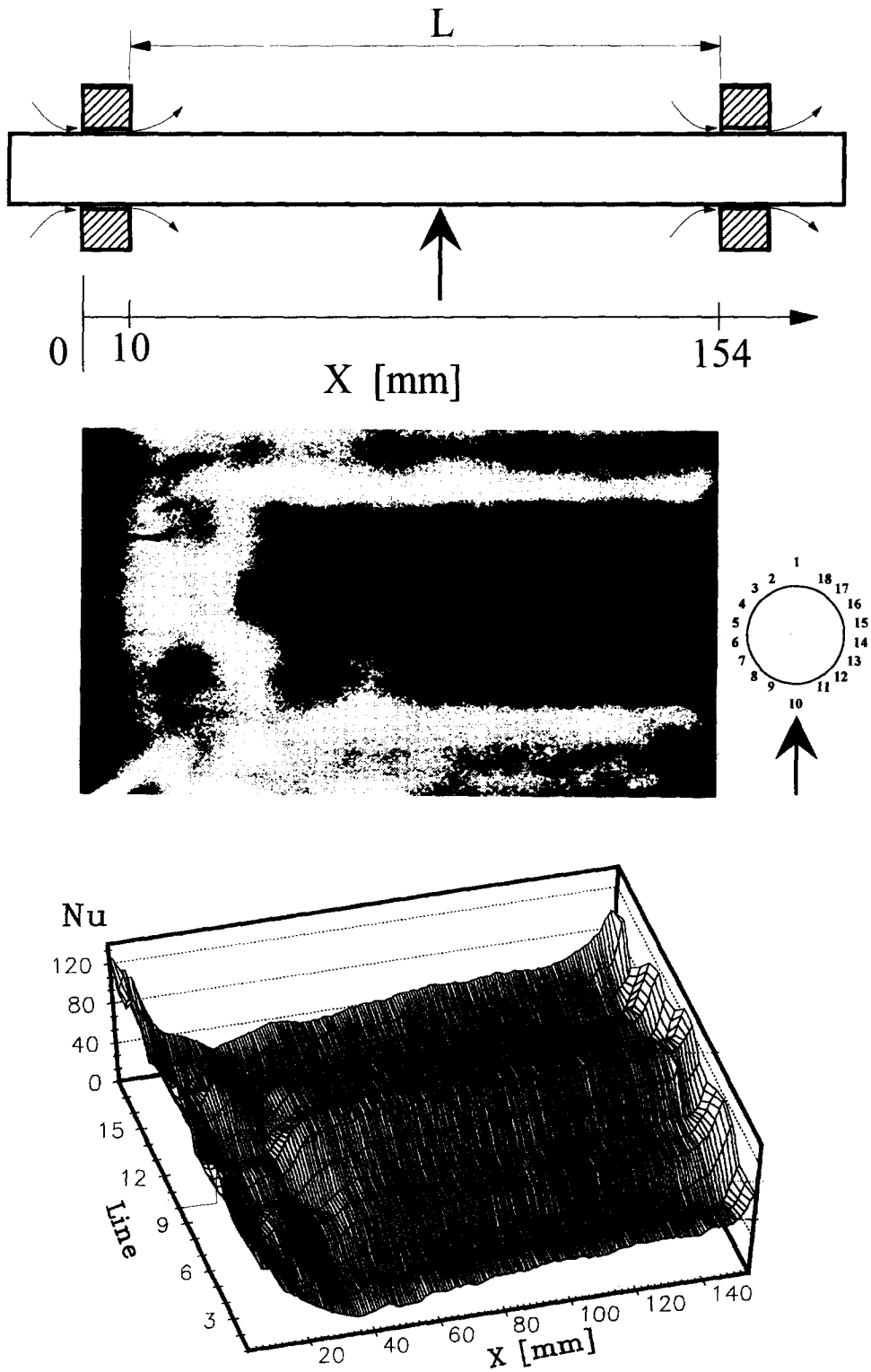

Fig. 2. Visualization and distribution of local mass and heat transfer on the surface of the tube 4.1 for $Re = 8000$ and $S = 144$ mm.

function of the Reynolds number. Compared with the predicted values from the *VDI-Wärmeatlas* [5] and from Gay [10], this figure shows a good agreement.

Pressure drop

Figure 6 shows that the baffle spacing affects also the pressure drop coefficient. In the experimental range of the Reynolds number, the pressure drop coefficient increases with the increase in baffle spacing, because of the higher flow velocity in the cross-flow zone as well as through the window at a larger baffle spacing. A good agreement between the results of this study and the values from the *VDI-Wärmeatlas* [6] can be observed for $Re > 3000$. This figure shows that the values in the VDI-Wärmeatlas are valid only for higher Reynolds numbers. An extension to lower Reynolds numbers needs new formulae.

Flow distribution

The fluid velocity u_0 through both the baffle-shell clearance and the baffle-tube clearance can be calculated from

$$u_0 = \sqrt{\frac{2\Delta P_2}{\rho \zeta_0}} \tag{1}$$

if the pressure drop ΔP_2 due to flow through these clearances and the pressure drop coefficient ζ_0 are known. According to Kukral [15], ζ_0 depends primarily on the orifice Reynolds number Re_0 and the orifice shape factor Z

$$Re_0 = u_0(D-d)/\nu \tag{2}$$

$$Z = 2\delta/(D-d) \tag{3}$$

$$\zeta_0 = a_1(Re_0, Z) + \frac{a_2(Z)}{Re_0^{a_3(Re_0, Z)}} \tag{4}$$

where D and d denote outer and inner diameter of the annular orifices in a plate of thickness δ, and a_1 to a_3 are functions of Re_0 and Z:

$$a_1(Re_0, Z) = \exp\left[a_{11}(Z)/(1+Re_0)^{a_{12}}\right] \tag{5}$$

$$a_{11}(Z) = a_{111} + a_{112}Z + a_{113}e^{-z} \tag{6}$$

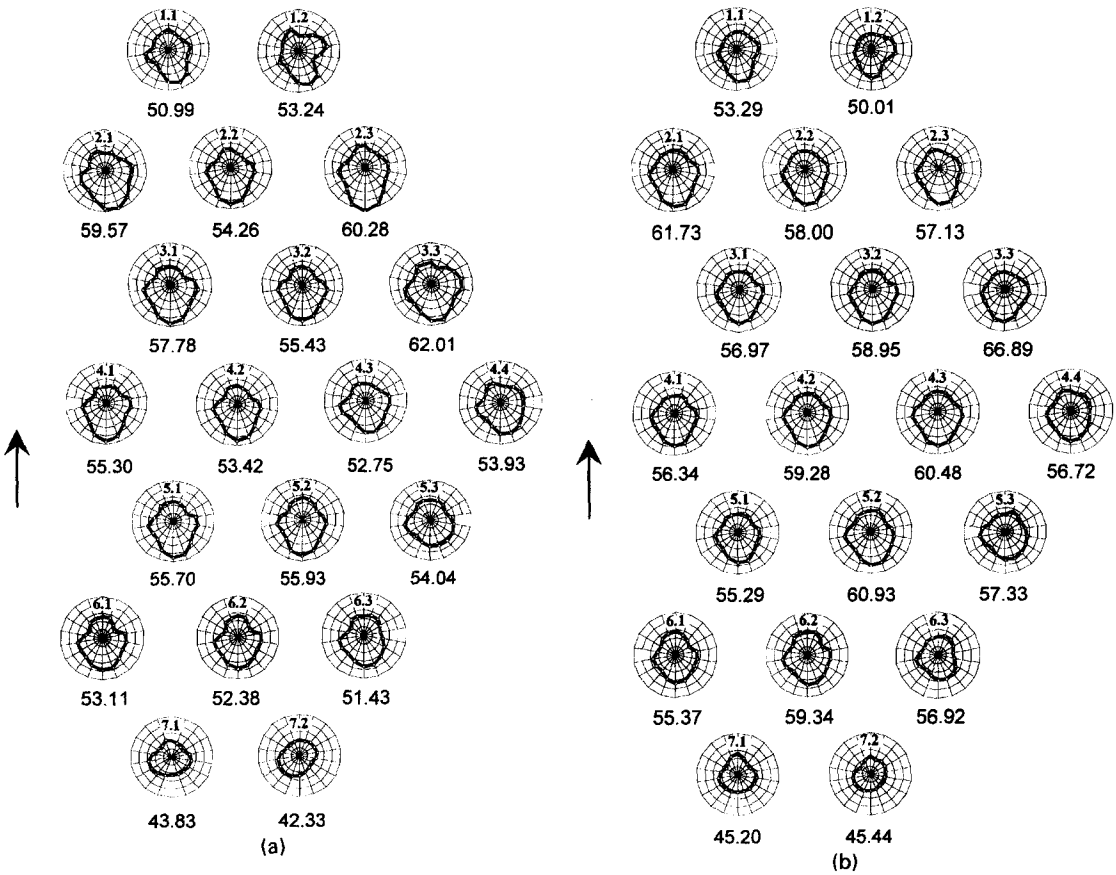

Fig. 3. (a) Circumferential distributions of the Nusselt numbers averaged over the tube length for $Re = 8000$ and $S = 113$ mm; (b) Circumferential distributions of the Nusselt numbers averaged over the tube length for $Re = 8000$ and $S = 144$ mm; (c) Circumferential distributions of the Nusselt numbers averaged over the tube length for $Re = 8000$ and $S = 175$ mm.

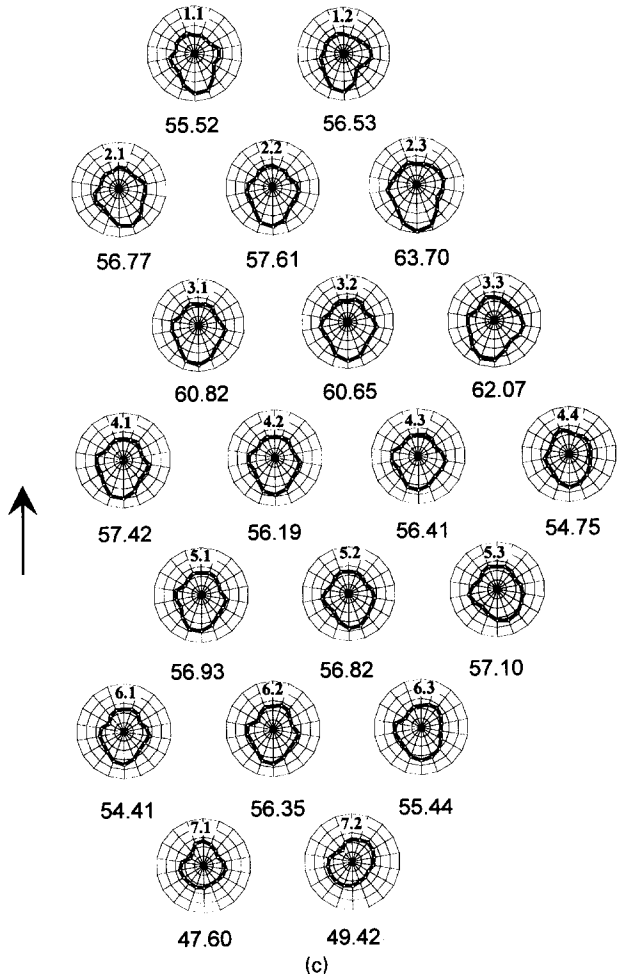

Fig. 3—*continued.*

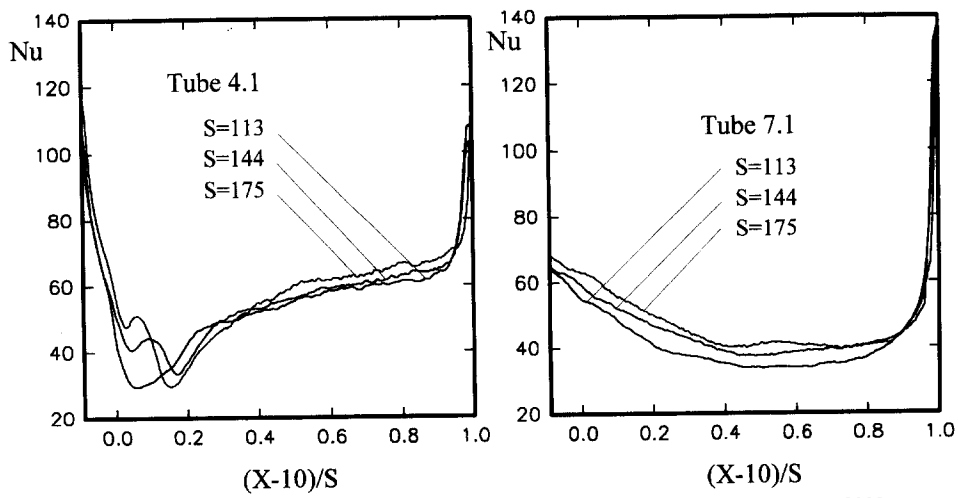

Fig. 4. Longitudinal profiles of the Nusselt number at the tubes 4.1 and 7.1 for $Re = 8000$.

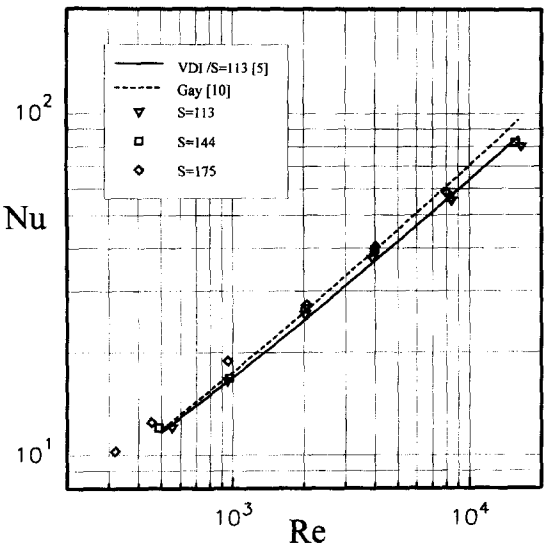

Fig. 5. Per-compartment Nusselt number in the tested baffle compartment.

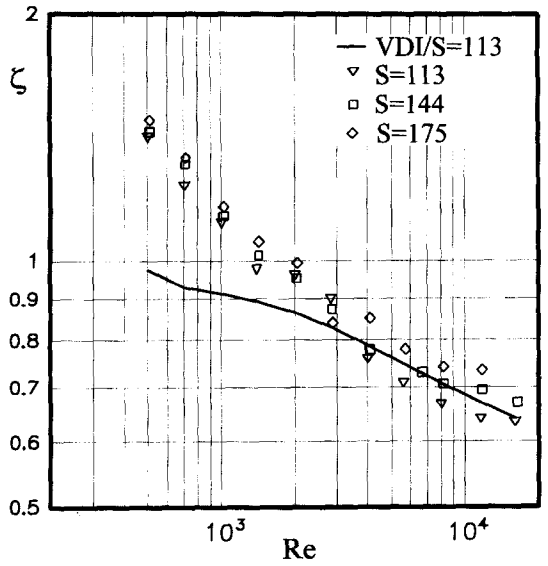

Fig. 6. Pressure drop coefficient in two baffle compartments.

$$a_2(Z) = a_{21} + a_{22}Z \tag{7}$$

$$a_3(Re_0, Z) = 1 + a_{31}Re_0/(1 + Re_0) \tag{8}$$

$$a_{31}(Z) = \max\{0,(4-Z)/12\} \tag{9}$$

The coefficients a_{111}, a_{112}, a_{113}, a_{12}, a_{21} and a_{22} can be taken from Table 2. Furthermore, in equations (4)–(8) Z must be set to $Z = 0.4$ if equation (3) yields values $Z < 0.4$.

In Fig. 7 the percentages of the main cross-flow stream at the three baffle spacings for $Re = 500$–16 000 are given relative to the volume flow rate at the entrance of the heat exchanger. The percentage of the main stream in the cross-flow zone of the fully developed baffle compartment (after the first-baffle-

Table 2. Coefficients for calculating the pressure drop coefficient for flow through annular orifices [15]

Coefficient	Orifice shape factor $0.1 \leqslant Z < 4$	$4 \leqslant Z \leqslant 30$
a_{111}	1.126	1.209
a_{112}	−0.156	0.0139
a_{113}	−0.251	4.744
a_{12}	0	0.125
a_{21}	64.51	16.59
a_{22}	13.54	19.12

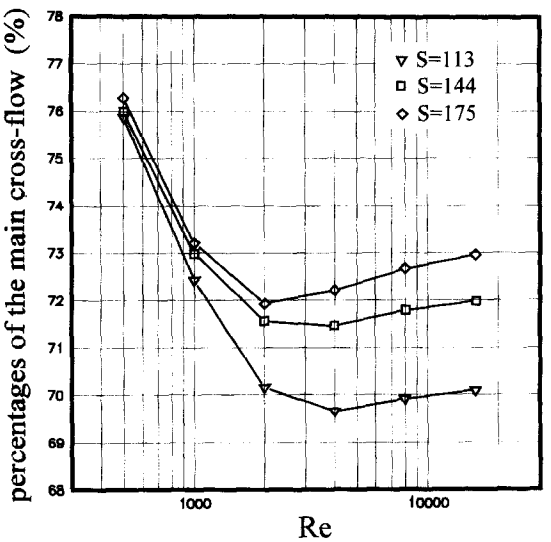

Fig. 7. Main cross-flow steam rate relative to volume flow rate at the entrance.

compartment [8]) depends on the baffle spacing and the Reynolds number. From $Re = 500$ to $Re = 2000$, the percentage of the main stream decreases. With further increase of the Reynolds number, it will slowly increase again, then keep constant.

In order to observe the detailed flow distribution, the percentages of the main stream and the leakages at $Re = 8000$ are presented in Figs. 8–10 for $S = 113$, 144 and 175 mm, respectively. Because of both higher pressure difference and the large baffle-shell clearance area, the most of the leakage concentrates in the roots of the baffle. Due to the reduction of the leakage percentage, the percentage of the main stream increases from $S = 113$ to $S = 175$ mm, which leads to the increase of the per-tube average Nusselt numbers in the cross-flow zone, as shown in Fig. 3.

In Fig. 11, the per-compartment average Nusselt number is presented as function of the effective Reynolds number Re_{eff}, which is based on the effective main flow rate in the cross-flow zone of a fully developed baffle compartment. The difference in Fig. 5 induced by the baffle spacing disappears in Fig. 11. The data for the three investigated baffle spacings can be correlated by an equation.

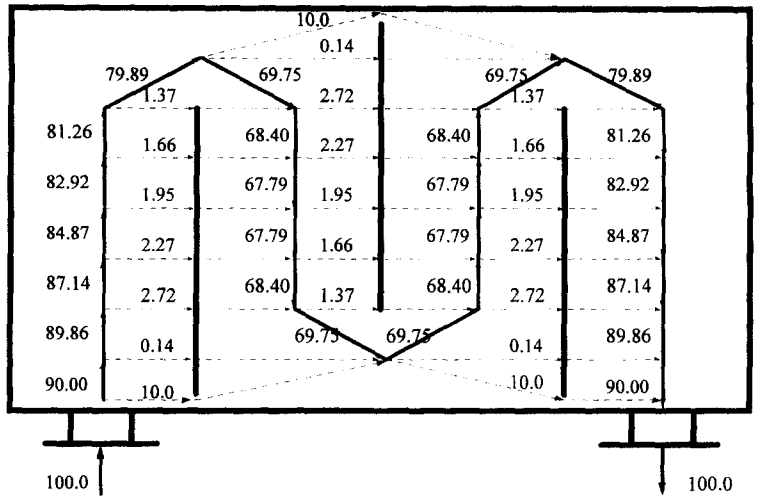

Fig. 8. Flow rates of main and leakage streams relative to the volume flow rate at the entrance for S 113 mm.

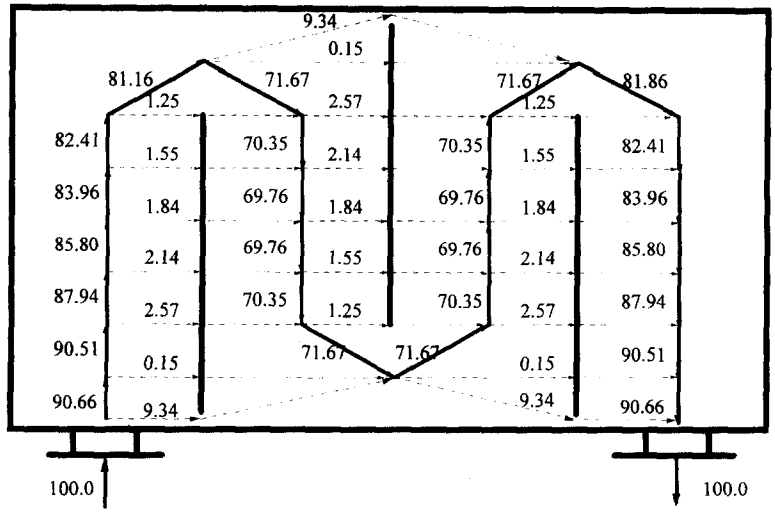

Fig. 9. Flow rates of main and leakage streams relative to the volume flow rate at the entrance for S 144 mm.

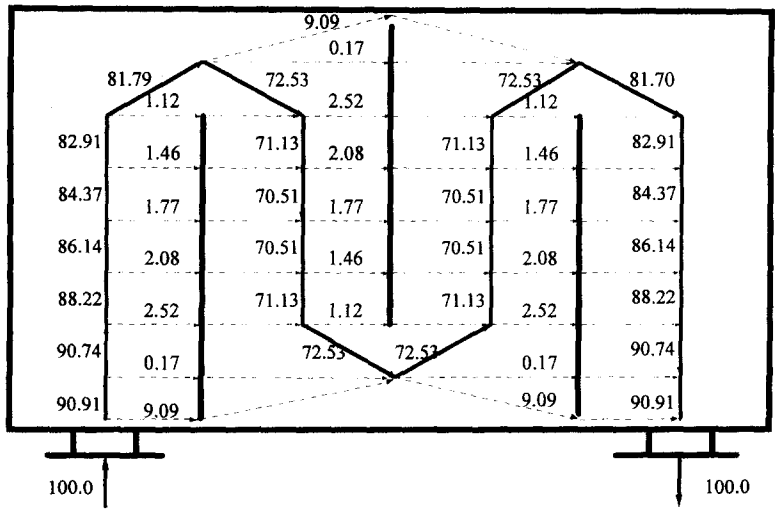

Fig. 10. Flow rates of main and leakage streams relative to the volume flow rate at the entrance for S = 175 mm.

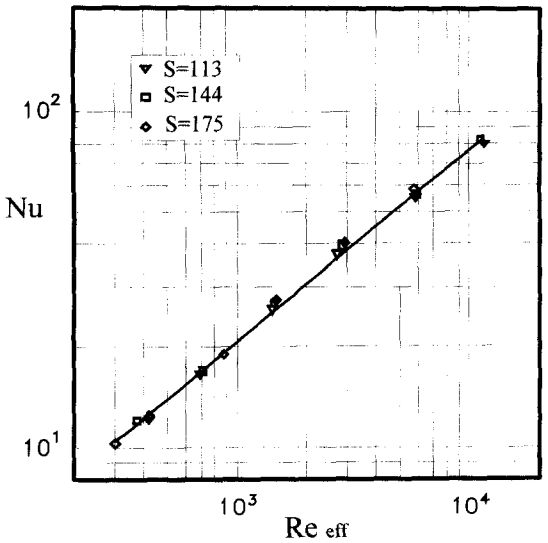

Fig. 11. Per-compartment Nusselt number as function of the effective Reynolds number.

$$Nu \propto Re_{\text{eff}}^{0.543} \tag{10}$$

CONCLUSIONS

An increasing baffle spacing can increase the heat transfer coefficient in the whole baffle compartment both due to the reduction of the percentage of the leakage stream and due to the higher flow velocity through the baffle opening. The local heat transfer coefficient distribution at an individual tube is slightly affected by the baffle spacing. The pressure drop coefficient for a long baffle spacing is higher than for a short one.

REFERENCES

1. Tinker, T., Shell side characteristics of shell and tube heat exchanger, Parts I, II, III, *General Discussion on Heat Transfer*. The Institution of Mechanical Engineers, 1951, pp. 89–116.
2. Bell, K. J., Final report of the cooperative research program on shell and tube heat exchangers. University of Delaware Engineering Experimental Station, Bulletin No. 5, 1963.
3. Donohue, D. A., Heat transfer and pressure drop in heat exchangers, *Industrial and Engineering Chemistry*, 1949, **41,** 53–60.
4. Palen, J. W. and Taborek, J., Solution of shell side flow pressure drop and heat transfer by stream analysis method. *Chemical Engineering Progress Symposium Series*, 1969, **92,** 53–63.
5. Gaddis, E. S. and Gnielinski, V., Wärmeübertragung im außenraum von rohrbündel-wärmeübertragern mit umlenkblechen. In *VDI-Wärmeatlas*, 6. Aufl., VDI, Düsseldorf, 1991, pp. Gg 1–6.
6. Gaddis, E. S., Druckverlust im außenraum von rohrbündel-wärmeübertragern mit und ohne einbauten. In *VDI-Wärmeatlas*, 6 Aufl., VDI, Düsseldorf 1991, pp. Lm 1–10.
7. Perez, J. A. and Sparrow, E. M., Determination of shell-side heat transfer coefficients by the naphthalene sublimation technique. *Heat Transfer Engineering*, 1985, **6**(2), 19–30.
8. Sparrow, E. M. and Reifschneider, L. G., Effect of interbaffle spacing on heat transfer and pressure drop in a shell-and-tube heat exchanger. *International Journal of Heat and Mass Transfer*, 1986, **29,** 1617–1628.
9. Gay, B., Mackley, N. V. and Jenkis, J. D., Shell-side heat transfer in baffled cylindrical shell-and-tube exchangers—an electrochemical mass-transfer modelling technique. *International Journal of Heat and Mass Transfer*, 1976, **19,** 995–1002.
10. Gay, B. and Roberts, P. C. O., Heat transfer on the shell-side of a cylindrical shell-and-tube heat exchanger fitted with segmental baffles, part II: flow patterns and local velocities derived from the individual tube coefficients. *Transactions of the Institution of Chemical Engineers*, 1970, **48,** T3–T6.
11. Kottke, V., Blenke, H. and Schmidt, K. G., Eine chemische farbreaktion zur messung örtlicher stoffübertragung und sichtbarmachung von strömungsvorgängen. *Wärme- und Stoffübertragung*, 1977, **10,** 9–21.
12. Kottke, V., A chemical method for flow visualization and determination of local mass transfer, flow visualization II. *Proceedings of the Second International Symposium on Flow Visualization*, Bochum, Germany, 1980, pp. 657–662.
13. Kottke, V., Blenke, H. and Schmidt, K. G., Messung und berechnung des örtlichen und mittleren stoffübergangs an stumpf angeströmten kreisscheiben bei unterschiedlicher trubulenz. *Wärme- und Stoffübertragung*, 1977, **10,** 89–105.
14. Nieva, I. A. and Böhm, U., Local mass transfer for cross flow through tube banks: equilateral triangular layout at intermediate Reynolds numbers. *International Committee of Heat and Mass Transfer*, 1985, **12,** 277–285.
15. Kukral, R. and Stephan, K., The effect of internal leakage on steady-state and transient behaviour of shell-and-tube heat exchangers. *Proceedings of 10th International Heat Transfer Conference*, Brighton, UK, 1994, pp. 395–398.